

Cite this: *Chem. Sci.*, 2025, 16, 21815

All publication charges for this article have been paid for by the Royal Society of Chemistry

## The air–water interfacial nitrogen cycle produces irrigatable-level ammonium nitrate

Xiaowei Song,<sup>a</sup> Chanbasha Basheer,<sup>b</sup> Jinheng Xu<sup>a</sup> and Richard N. Zare<sup>\*a</sup>

We report a sustainable, air-based strategy for synthesizing ammonium nitrate ( $\text{NH}_4\text{NO}_3$ ) by harnessing the redox-active properties of microscale air–water interfaces. The process proceeds through two sequential reactions: (1) the nitrogen oxidation reaction (NOR), generating nitrate ( $\text{NO}_3^-$ ) from atmospheric  $\text{N}_2$ , and (2) the nitrate reduction reaction ( $\text{NO}_3\text{RR}$ ), converting nitrate into ammonium ions ( $\text{NH}_4^+$ ). In the first step, ambient air is introduced into a recirculating microbubble system, where solar irradiation and a water-soluble photocatalyst drive the efficient oxidation of  $\text{N}_2$  to nitrate, producing  $\text{NO}_3^-$  at a rate of  $500 \mu\text{mol L}^{-1} \text{h}^{-1}$ . In the second step, atomized water microdroplets are sprayed across a  $\text{Fe}_3\text{O}_4$ –Nafion–CuO mesh, generating an extensive air–water interfacial area that promotes the reduction of nitrate and nitric oxide intermediates to  $\text{NH}_4^+$ . Over 12 hours, this tandem process yields a 50 mL aqueous solution containing 0.94 mM  $\text{NH}_4\text{NO}_3$  and 4.42 mM  $\text{HNO}_3$ , derived entirely from air and water. This carbon-free and catalyst-assisted platform offers a decentralized and environmentally friendly approach to nitrogen fixation, with immediate applications in hydroponic systems, where controlled nutrient delivery is essential. The integration of solar photocatalysis with microdroplet interfacial chemistry establishes a viable foundation for next-generation green fertilizer technologies.

Received 30th July 2025  
Accepted 14th October 2025

DOI: 10.1039/d5sc05754j

rsc.li/chemical-science

### Introduction

Ammonia plays a fundamental role in building life and supporting modern human society. It is one of the most important fertilizers for providing nitrogen sources, which is indispensable for basic life building blocks such as amino acids and nucleotides. With the invention of the Haber–Bosch process (HBP) for industrial ammonia synthesis in the early 20th century, world food production surged sharply, accompanied by a significant increase in human population.<sup>1,2</sup> Unfortunately, this classical ammonia production method begins with nitrogen and hydrogen derived from the steam reforming of methane gas. The harsh conditions (15–25 MPa and 400–500 °C) require an intensive energy input and account for approximately 1–2% of global energy consumption.<sup>3,4</sup> HBP is also responsible for a substantial portion of industrial greenhouse gas emissions, given that it often relies on fossil fuels, particularly natural gas, for both hydrogen production and as an energy source.<sup>5</sup> Efforts to reduce the carbon footprint of HBP include exploring alternative hydrogen sources and efficient catalytic strategies for the nitrogen reduction reaction (NRR) at lower temperatures and pressures.<sup>6</sup>

Water is the ideal hydrogen resource compared to methane because it is carbon-free, clean, widely available, and renewable in nature. Compared to bulk water, numerous studies have demonstrated that micron-sized droplets can serve as highly active reactors for both oxidation and reduction.<sup>7–15</sup> It can not only be a source of reducing species but also a source of reactive oxygen species, which have also been observed across the air–water interface of microdroplets in many showcase experiments.<sup>16–21</sup> Apart from water microdroplets, some research study also observed the generation of hydrogen peroxide ( $\text{H}_2\text{O}_2$ ) and hydroxyl radicals ( $\text{OH}^\bullet$ ) at another reversed form of air–water interface of electrogenerated microbubbles on an electrode surface.<sup>22,23</sup> Regardless of whether it is microdroplets or microbubbles, the large gas-contact area and redox potential of the air–water interface region provide a promising 2D environment for nitrogen fixation.

Previously, we successfully identified the formation of ammonia by spraying  $\text{N}_2$  with water microdroplets through a copper oxide (CuO) mesh coated with a catalyst ( $\text{Fe}_3\text{O}_4$ –Nafion). The ammonia generated can reach a concentration of 60  $\mu\text{M}$  within 1 hour of operation under ambient conditions.<sup>24</sup> Later, a more efficient device was developed to conduct on-site ammonia synthesis using water vapor and dinitrogen in the air as the feedstock. The ammonia concentration increased to  $270.2 \pm 25.1 \mu\text{M}$  after 2 hours of operation, which is sufficient for some agricultural irrigation purposes.<sup>25</sup> We also detected  $\text{NO}_3^-$  generation during the microdroplet spraying process. The air–water interfacial hydroxyl radicals lead to the oxidation of

<sup>a</sup>Department of Chemistry, Stanford University, CA, 94305, USA. E-mail: zare@stanford.edu

<sup>b</sup>Chemistry Department, King Fahd University of Petroleum and Minerals, Dhahran, 31261, Saudi Arabia. E-mail: cbasheer@kfupm.edu.sa



either  $N_2$ <sup>26–29</sup> or the generated  $NH_3$ .<sup>30,31</sup> This observation further supported the fact that the water microdroplet interface may have an asymmetric redox ability to conduct both nitrogen reduction and oxidation, which formed ammonium nitrate ( $NH_4NO_3$ ) as the actual product during our previous ammonia synthesis from the nitrogen in air.

Inspired by the intermolecular conversion cycle composed of  $N_2$ ,  $NO_3^-$ , and  $NH_4^+$ , we are motivated to take advantage of the redox process of the micron-sized air–water interfacial environment for nitrogen fixation. A sequential process was conducted including the first step of the nitrogen oxidation reaction (NOR) that converts  $N_2$  to  $NO_3^-$  in a circulating microbubble system, followed by the nitrate reduction reaction ( $NO_3RR$ ) that partially converts the  $NO_3^-$  into  $NH_4^+$  in a spraying microdroplet system, resulting in  $NH_4NO_3$  and extra  $HNO_3$  as final aqueous products.

## Results

### Highly efficient oxidation of nitrogen by microbubbles of air in water

The first step of our method is to oxidize the nitrogen in the air into nitrate. We developed a dinitrogen-to-nitrate reactor assembly to achieve this goal. This device mainly consists of a microbubble generator, a nitrogen oxidation reactor, and a reactive oxygen species (ROS) enhancer (Fig. 1). The microbubble generator can effectively increase the surface-to-volume ratio of the bulk water and contacting area of the air–water interface, which has been proven to be a highly reactive region rich in ROS, such as hydroxyl radical ( $OH^\bullet$ ), superoxide anion ( $O_2^{\bullet-}$ ), and hydrogen peroxide ( $H_2O_2$ ).<sup>32,33</sup> Nitrogen in the air can be fully dispersed into bulk water to maximize the exposure of nitrogen to the active interfacial region and extend the oxidation period.

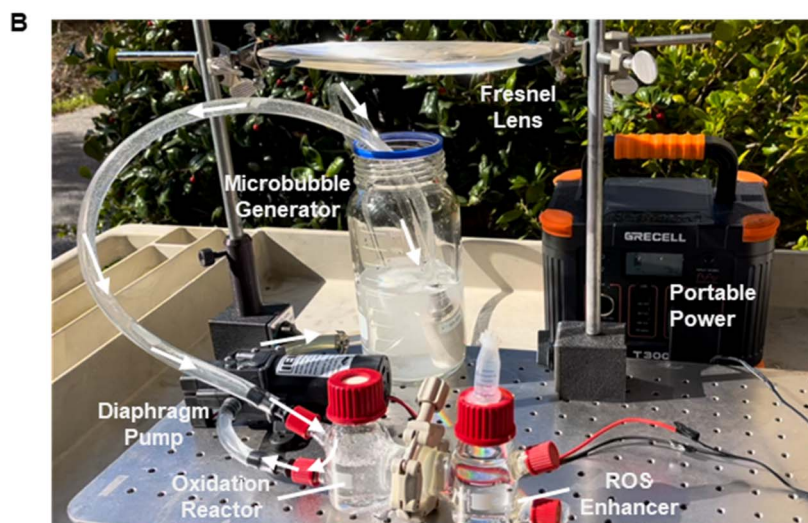
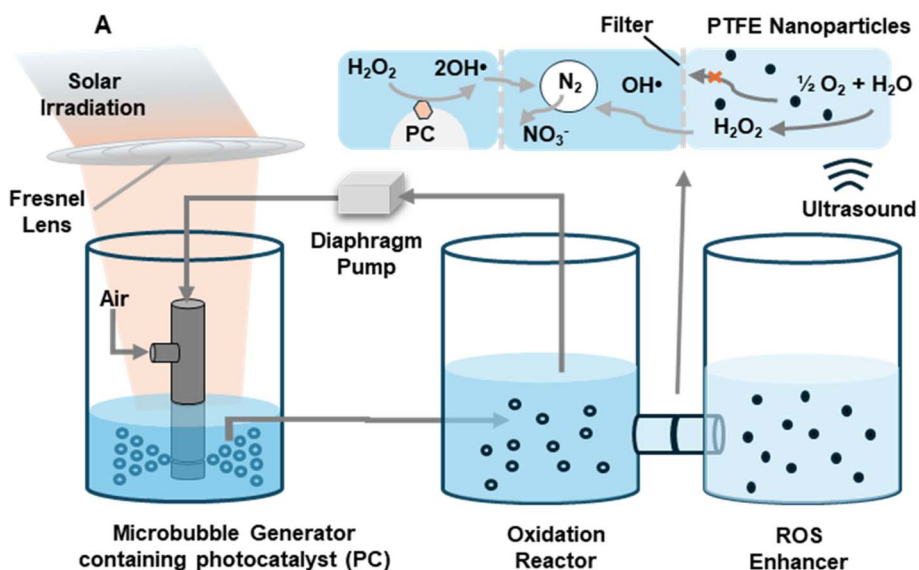


Fig. 1 A continuous microbubble system for nitrogen oxidation to nitrate. (A) Schematic illustration of the setup, which consists of a microbubble generator, an oxidation reactor, and an additional ROS enhancer. (B) Photograph of the real microbubble setup working outdoors, driven by a portable power supply under natural sunlight irradiation.



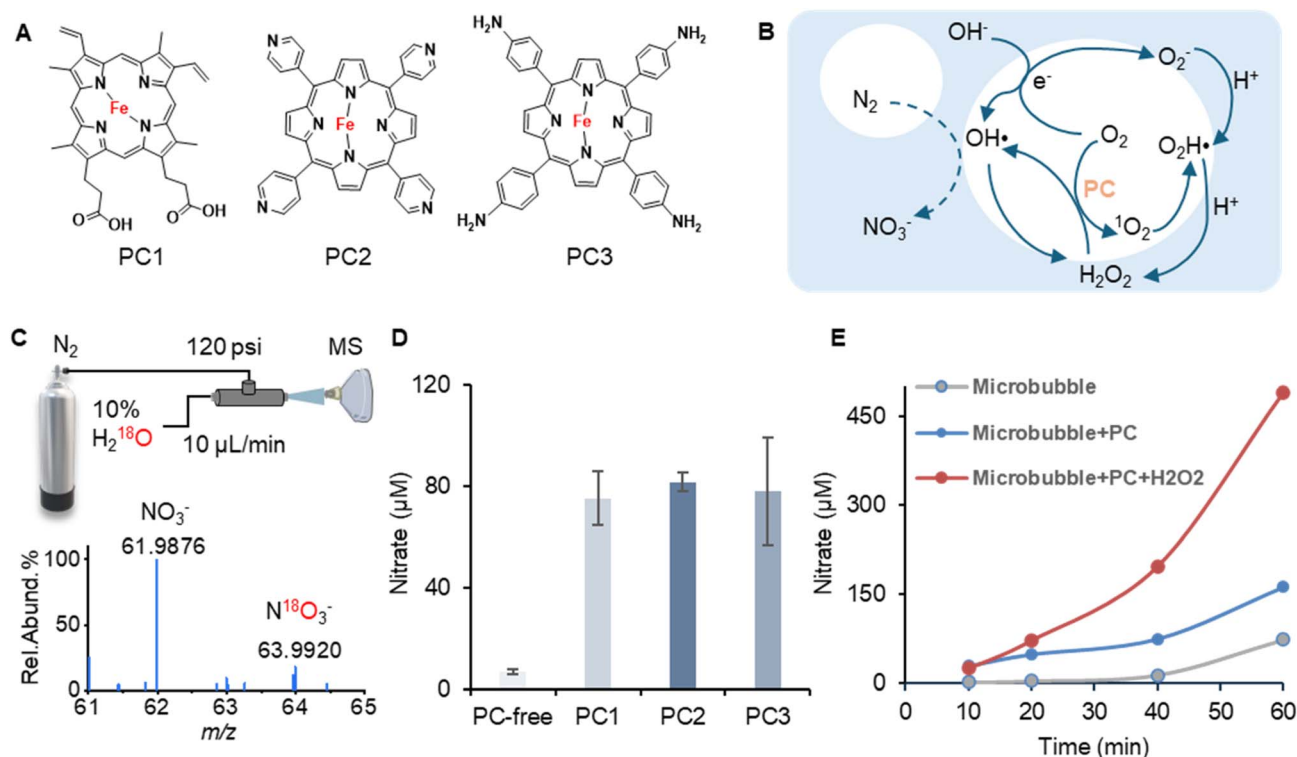


Fig. 2 Investigating nitrogen oxidation and final nitrate production facilitated by the photocatalyst and externally generated  $\text{H}_2\text{O}_2$  by contact-electrocatalysis. (A) Chemical structures of three different photocatalysts (PC); (B) diagram of the reactive oxygen species interconversion facilitated by PC and the air–water interface; (C) high-resolution mass spectrometry confirmation of the hydroxyl radical-involved nitrate generation by using native water spiked with 10%  $^{18}\text{O}$ -labelled water; (D) the improvement of nitrate production by adding different types of photocatalysts in the microbubble system; (E) the improvement of nitrate production with time by adding  $\text{H}_2\text{O}_2$  externally generated from the ROS enhancer unit.

To further enhance the efficiency of the nitrogen oxidation process, an optional ROS enhancer can be coupled with a microbubble generator and an oxidation reactor. The generated microbubbles can be transported to the oxidation reactor to fully interact with the  $\text{H}_2\text{O}_2$  generated from the reactive oxygen species (ROS) enhancer unit. The ROS enhancer is filled with deionized water with polytetrafluoroethylene (PTFE) nanoparticles dispersed inside. An additional amount of 300  $\mu\text{M}$   $\text{H}_2\text{O}_2$  can be produced by ultrasonating the enhancer unit for 1 hour in advance before running the microbubble generator.<sup>34,35</sup> This extra 300  $\mu\text{M}$   $\text{H}_2\text{O}_2$  can freely diffuse into the neighboring oxidation reactor and reach an equilibrium within 2 hours (Fig. S1), leading to the enhancement of the nitrogen to nitrate conversion across the interfacial region. The ultrafiltration film embedded between the oxidation unit and enhancer unit can block the PTFE particles from diffusion and clogging in the diaphragm pump and narrow channel within the microbubble generator.

The  $\text{OH}^\bullet$  around the air–water interface can be formed through multiple ways by interacting with the surrounding air. First, the  $\text{OH}^\bullet$  can directly come from  $\text{OH}^-$  by losing one electron, which is thermodynamically favorable across the air–water interface based on the theoretical calculation.<sup>36</sup> Second, the  $\text{OH}^\bullet$  can be indirectly generated from  $\text{H}_2\text{O}_2$  in the presence of oxygen ( $\text{O}_2$ ), protons, and solvated electrons. It has been discovered that air–water interfaces can not only induce the generation of

$\text{O}_2^-$ , hydroperoxyl radical ( $\text{OOH}^\bullet$ ), and singlet oxygen ( $^1\text{O}_2$ ) but also promote the photocatalysis process.<sup>37–41</sup> In this study, three water-soluble iron porphyrins were also investigated in the microbubble circulating system (Fig. 2A). Iron porphyrins can serve as photocatalysts (PCs) to break  $\text{H}_2\text{O}_2$  into active  $\text{OH}^\bullet$  under solar light irradiation. Singlet oxygen can also be generated by the photocatalyst upon light excitation. All these species can promote the  $\text{OH}^\bullet$  formation by interacting with the water molecules through different pathways.

As shown in Fig. 2C, during a 30-minute operation, the average concentration ( $n = 3$ ) of nitrate increases from 6.7  $\mu\text{M}$  to 74.9  $\mu\text{M}$  (PC1), 81.5  $\mu\text{M}$  (PC2), and 77.9  $\mu\text{M}$  (PC3) with the addition of PC in the microbubble system, respectively. The device can achieve an even better performance when using the ROS enhancer. Within 1 hour of operation, the nitrate concentration can reach 489.5  $\mu\text{M}$  with the use of the extra ROS enhancer plus PC2 group compared to 162.1  $\mu\text{M}$  for the PC2 group and 73.9  $\mu\text{M}$  for the microbubble alone group (Fig. 2D).

### Air–water interfacial nitrogen cycle

Our previous studies have already demonstrated that ammonia can be formed by spraying water microdroplets and dinitrogen through the catalyst-coated mesh ( $\text{Fe}_3\text{O}_4\text{-Nafion@CuO}$ ).<sup>24,25</sup> Both ammonia and dinitrogen gas can also be directly oxidized into nitrates by spraying microdroplets.<sup>26–31</sup> These facts indicate



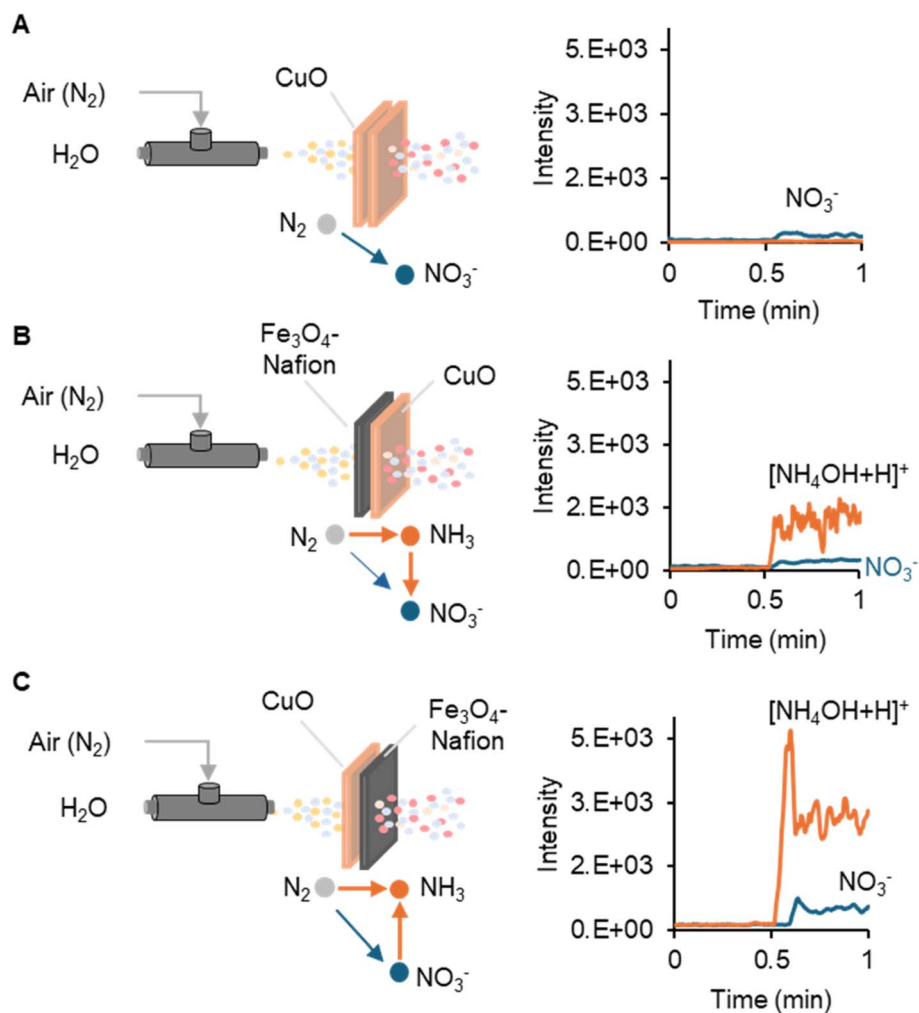


Fig. 3 Online mass spectrometry monitoring nitrogen oxidation and reduction products after spraying water microdroplets and air through different types of metal oxide meshes: (A) double layers of CuO meshes; (B)  $\text{Fe}_3\text{O}_4$ -Nafion-coated CuO mesh in the front and another CuO mesh in the back; (C) CuO mesh in the front and  $\text{Fe}_3\text{O}_4$ -Nafion-coated CuO mesh in the back.

an air–water interfacial nitrogen cycle composed of dinitrogen, ammonia, and nitrate species.

Because nitrate reduction into ammonia is a more effective way requiring less energy-cost compared to direct reduction of dinitrogen gas,<sup>42–44</sup> we are motivated to explore the new path of ammonia production further, starting from nitrate. We use a classical coaxial capillary atomizer to generate a water microdroplet spray with the aid of compressed air (100 psi) as the nebulizing gas (Fig. 3). A linear ion trap mass spectrometry was employed to monitor the nitrogen species and their changes.

When we let spraying water microdroplets and air pass through the CuO mesh, the ion intensity of  $m/z$  62 ( $\text{NO}_3^-$ ) was doubled from  $7.2 \times 10^1$  to  $1.8 \times 10^2$  (Fig. 3A). This phenomenon indicates the enhancement of nitrogen oxidation with the involvement of a CuO mesh, which serves as a Fenton-like catalyst.<sup>30</sup> When another  $\text{Fe}_3\text{O}_4$ -Nafion@CuO mesh was stacked in front of the CuO mesh for interacting with the microdroplet spray, the ion intensity of  $m/z$  36 had a sharp surge from  $6.8 \times 10^1$  to  $1.5 \times 10^3$ , indicating the generation of ammonia ( $[\text{NH}_4\text{OH} + \text{H}]^+$ ) from dinitrogen gas. Meanwhile, the

$\text{NO}_3^-$  ion at  $m/z$  62 also reached a level of  $2.3 \times 10^2$  (Fig. 3B), which is slightly higher than what we observed when spraying through the CuO mesh alone. This is because although both  $\text{N}_2$  and  $\text{NH}_3$  can contribute to  $\text{NO}_3^-$  formation,  $\text{NH}_3$  is more readily oxidized than  $\text{N}_2$ . Finally, when we reversed the  $\text{Fe}_3\text{O}_4$ -Nafion/CuO (back) and CuO (front) meshes, the ion intensity of  $m/z$  36, representing  $[\text{NH}_4\text{OH} + \text{H}]^+$ , increased to  $2.9 \times 10^3$ , compared to the previous value of  $1.5 \times 10^3$  (Fig. 3C). This result supports our hypothesis that converting  $\text{N}_2$  to  $\text{NO}_3^-$  as the first step can effectively improve the subsequent nitrogen reduction into  $\text{NH}_3$ . It is worth noting that the ion intensity of  $m/z$  62 representing  $\text{NO}_3^-$  also further increased to  $5.1 \times 10^2$  compared to the previous  $2.3 \times 10^2$  level. This may suggest that  $\text{NO}_3^-$  is also a possible byproduct from unavoidable  $\text{NH}_3$  oxidation.

#### Critical nitrogen species showing the ongoing NO<sub>3</sub>RR to form ammonia

An Orbitrap high-resolution mass spectrometer (HRMS) was employed to gain a deep insight into the stepwise NORR process in the negative scanning mode. When directly spraying the air



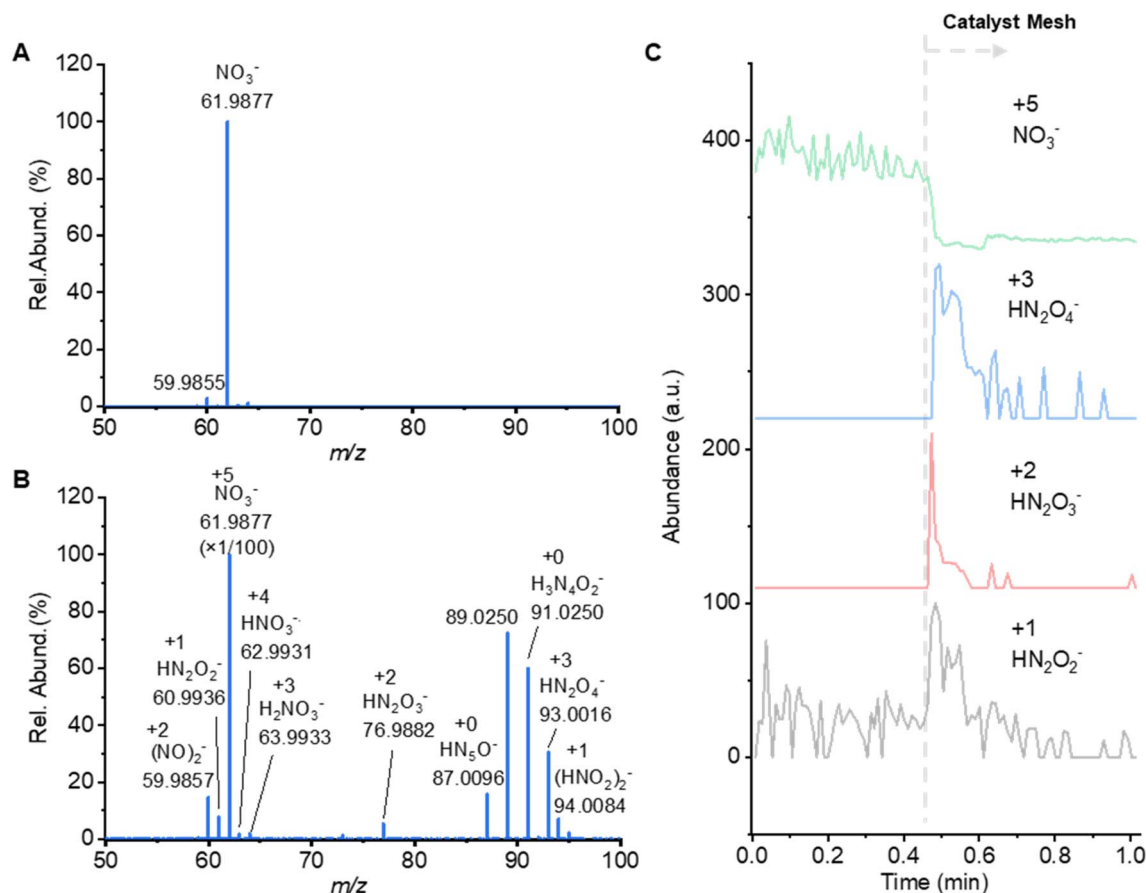


Fig. 4 Characterizing valence changes of the nitrogen element from stepwise hydrogenation during the nitrate reduction process. (A) The mass spectrum was collected in negative mode by spraying water microdroplets containing nitrate sodium directly into the mass spectrometer. (B) The mass spectrum was acquired by spraying water microdroplets containing sodium nitrate through the  $\text{CuO}$  mesh coated with the  $\text{Fe}_3\text{O}_4$ -Nafion catalyst. (C) Extracted ion chromatograms of nitrate and representative  $\text{NO}_x^-$  species with reduced valence.

and water, a strong peak at  $m/z$  61.9877 ( $\text{NO}_3^-$ ) can be detected (Fig. 4A). When the  $\text{Fe}_3\text{O}_4$ -Nafion@ $\text{CuO}$  mesh was mounted in the middle of the nozzle atomizer and the MS inlet, a set of associated peaks appeared in the mass spectrum. Exploring elemental compositions, they can be putatively annotated as various  $\text{N}_x\text{O}_y\text{H}_z$  species. Although the detailed molecular structure cannot be elucidated by the HRMS alone, the elemental composition information is sufficient to clarify the valence profile of these  $\text{N}_x\text{O}_y\text{H}_z$  species, which varied from +5 ( $m/z$  61.9877,  $\text{NO}_3^-$ ) to +4 ( $m/z$  62.9931,  $\text{HNO}_3^-$ ), +3 ( $m/z$  63.9933,  $\text{H}_2\text{NO}_3^-$ , and  $m/z$  93.0016,  $\text{HN}_2\text{O}_4^-$ ), +2 ( $m/z$  76.9882,  $\text{HN}_2\text{O}_3^-$ ), +1 ( $m/z$  61.0040,  $\text{HN}_2\text{O}_2^-$ ) (Fig. 4B). Although the  $\text{NO}_3^-$  peak at  $m/z$  61.9877 remained the base peak, its signal strength immediately dropped by 80% (Fig. 4C). In contrast, these  $\text{N}_x\text{O}_y\text{H}_z^-$  species were only present and appeared when the catalyst mesh was mounted in front of the spray. The apparent valence changes from +5 to +1 indicate the ongoing stepwise hydrogenation and reduction processes.

### Theoretical calculation for ammonia synthesis from the $\text{NO}_3\text{RR}$

We further conducted theoretical computations on the stepwise interaction between the catalytic center and the  $\text{N}_x\text{O}_y\text{H}_z^-$

species, molecular structure changes, and the corresponding potential energy landscape across the entire  $\text{NO}_3\text{RR}$  process using density functional theory (DFT) calculations. The crystal face of (311) of  $\text{Fe}_3\text{O}_4$  was selected for nitrate adsorption and activation because it was confirmed to be the major form by X-ray diffraction (XRD) (Fig. S3). Throughout the interaction diagram shown in Fig. 5A, the change of nitrogen valence from +5 to +1 is consistent with the captured  $\text{N}_x\text{O}_y\text{H}_z^-$  species in the HRMS experiment.

Regarding the potential energy change, after one  $\text{NO}_3^-$  molecule was chemically adsorbed to the ferrous center by forming two Fe-O coordination bonds, one Fe-O bond will be liberated by adding a  $\text{H}^+$  donated from water microdroplets. This is the first rate-limiting step with the highest activation energy (3 eV) across the whole process because one of the Fe-O bonds needs to be liberated to make the oxygen available to accept the donated proton. Thereafter, stepwise hydrogenation can spontaneously proceed without overcoming any energy barrier until the step of  $(\text{NO})_{\text{ads}}$  reduction into  $(\text{HNO})_{\text{ads}}$ . This is the second rate-limiting step with a relatively high energy barrier around 1.07 eV, and all the other steps are energetically downhill (Fig. 5B).



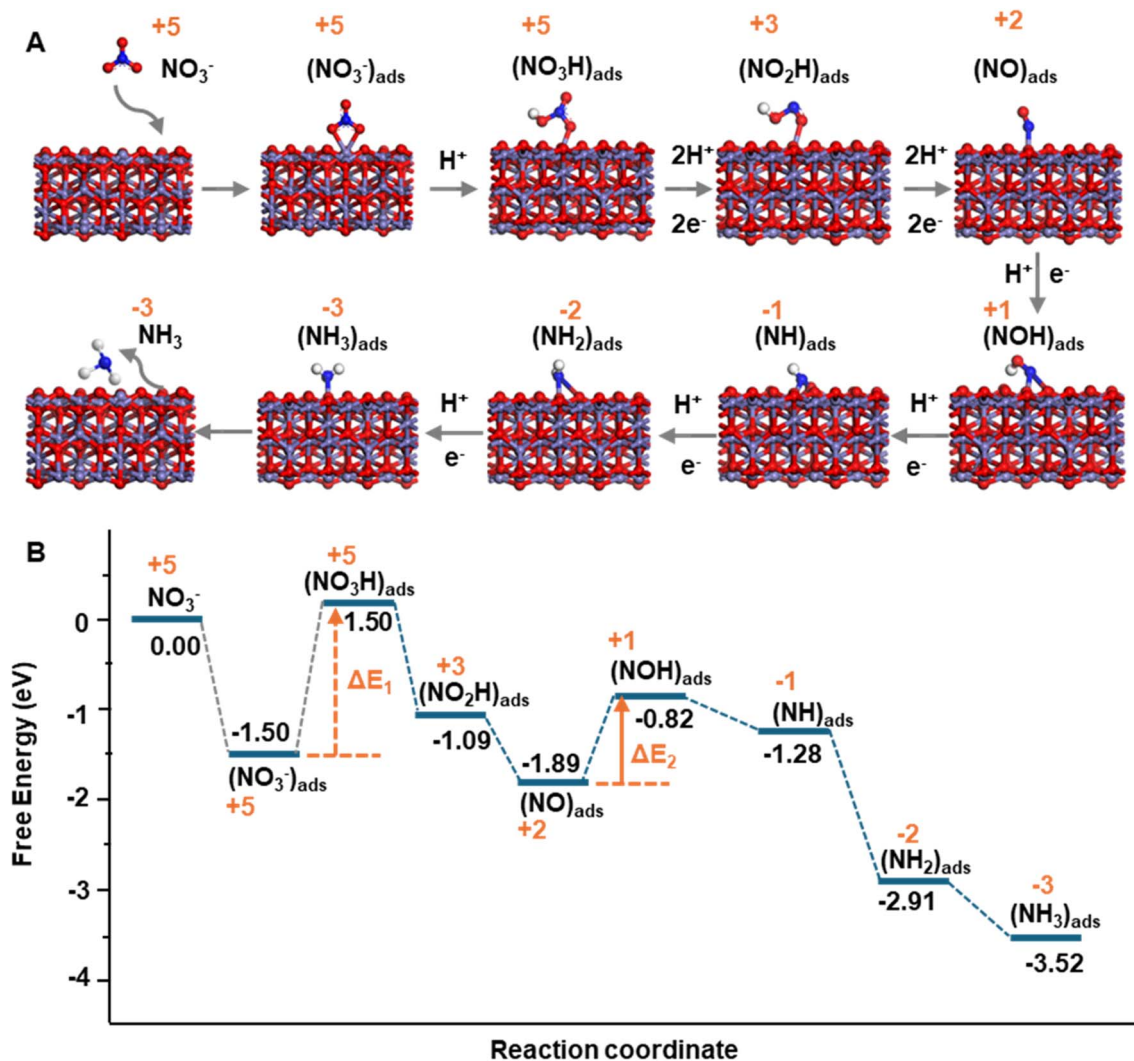


Fig. 5 DFT calculation of nitrate reduction into ammonia. (A) Diagram of the nitrate molecule absorption and stepwise hydrogenation across the Fe<sub>3</sub>O<sub>4</sub> surface; (B) energy changes during the whole nitrate reduction process.

Previous studies have demonstrated that spraying water microdroplets can not only cause contact electrification at the water–metal mesh interface<sup>45–48</sup> but also induce microlightning during droplet splitting.<sup>49</sup> The microlightning of microdroplets can ionize the surrounding molecules, even those relatively inert molecules such as xenon (ionization energy around 12 eV). The negative contact electrified potential between microdroplets and catalyst mesh can provide the driving force to overcome the energy barriers of the two steps. The contact electrified potential was also attributed to the use of Nafion whose hydrophobic perfluoroalkyl backbone can accept, stabilize, and facilitate reducing electrons to transfer from the microdroplet surface to the N<sub>x</sub>O<sub>y</sub>H<sub>z</sub><sup>-</sup> species. The sulfonic acid group in the Nafion film can also facilitate the reduction by H<sup>+</sup> transfer. Our previous HRMS test successfully captured the *m/z* 62.9931 (HNO<sub>3</sub><sup>-</sup>) and *m/z* 61.0040 (HN<sub>2</sub>O<sub>2</sub><sup>-</sup>) ions, which represent the nitrogen valences of +5 and +1, respectively. This provides evidence that these two critical steps can be achieved in the microdroplet interfacial catalysis process.

### Highly efficient nitrate reaction to ammonia at the air–water interface

After achieving the oxidation of N<sub>2</sub> to NO<sub>3</sub><sup>-</sup> in microbubbles and reduction of NO<sub>3</sub><sup>-</sup> to NH<sub>3</sub> in microdroplets, we combined these two steps sequentially to maximize the ammonium nitrate production. We first ran the microbubble reactor described above for 12 hours to produce approximately 6.3 mM nitrate in 50 mL solution. Then, the 50 mL nitrate solution was transferred into a scaled-up nozzle atomizer embedded with the Fe<sub>3</sub>O<sub>4</sub>–Nafion@CuO catalyst mesh, a nozzle atomizer for continuous spraying, and a peristaltic pump for water solution circulation (Fig. 6A). Finally, 0.94 mM ammonia can be produced within only 1 hour of running (Fig. 6B). Given the unreacted nitrate in the solution, there was 0.94 mM ammonium nitrate and an additional 4.42 mM nitrate produced in total over 13 hours of operation. This concentration is sufficient for direct irrigation purposes.<sup>50,51</sup> Additionally, we found that the solution pH is a critical factor that affects the ammonia production efficiency. A pH of 1.0–2.0 can achieve near-mM level production, whereas



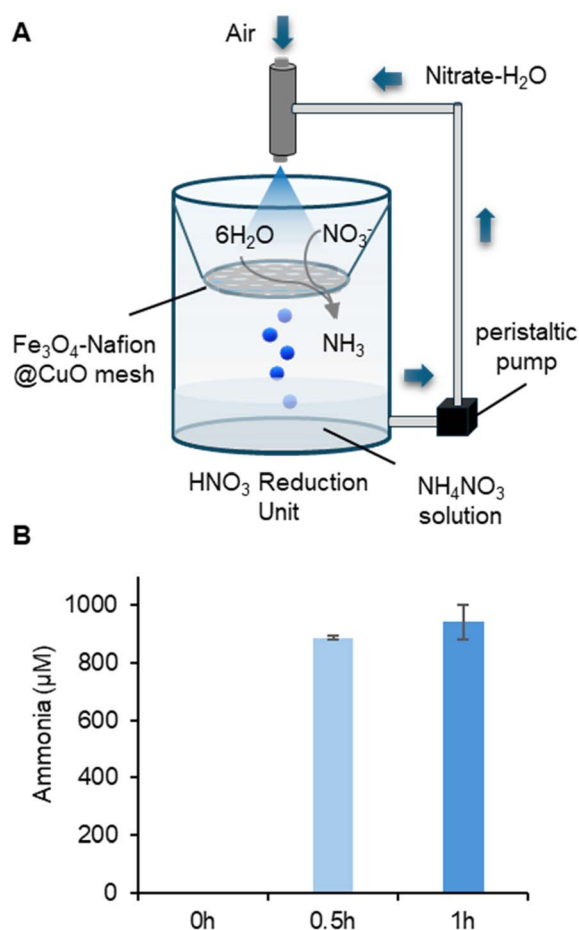


Fig. 6 Ammonia production utilizes nitrate as the starting material. (A) Diagram of the scaled-up setup equipped with a 100 mL volume reactor embedded with the  $\text{Fe}_3\text{O}_4\text{-Nafion@CuO}$  catalyst mesh, a nozzle atomizer for continuous spraying, and a peristaltic pump for water solution circulation. (B) The mM level of ammonia production with a 1-hour operation feed with a nitrate solution.

a pH higher than 2.0 can only achieve a concentration of 147–188  $\mu\text{M}$  ammonium nitrate (Fig. S4). Nonetheless, even the 147–188  $\mu\text{M}$  ammonium nitrate plus the unreacted 6.2 mM nitrate is still suffice for the irrigation, regardless of whether nitrogen element is present in the form of ammonia or nitrate.

The stability of the  $\text{Fe}_3\text{O}_4\text{-Nafion-CuO}$  catalyst was first investigated by mounting in front of sprayed microdroplets and nebulizing the gas for 1 hour of continuous running. The produced ammonia ion intensity gradually drops to a relatively stable level after 30 minutes (Fig. S5A). Thereafter, the activity of the catalyst during the long-term storage was tested by successively using the same catalyst mesh at 1, 7, 14, 21, and 30 days after the preparation. As a result, the catalyst can retain the active performance for at least two weeks when stored at room temperature and in an open environment (Fig. S5B).

## Discussion

Our study has demonstrated how to more effectively utilize a micron-sized air-water interfacial environment to convert  $\text{N}_2$

into  $\text{NH}_4\text{NO}_3$ , a commonly used fertilizer in agriculture. By integrating two reactions into a closed-loop nitrogen system where atmospheric  $\text{N}_2$  is first oxidized to  $\text{NO}_3^-$  and then reduced to  $\text{NH}_3$ , the process effectively emulates natural nitrogen cycling. This tandem approach offers a sustainable pathway for decentralized fertilizer production, reduces greenhouse gas emissions, and aligns with the principles of green chemistry and a circular economy.

Compared to dinitrogen,  $\text{NO}_3^-$  is a better alternative nitrogen source. Compared to the NRR, the  $\text{NO}_3\text{RR}$  offers a cost-effective strategy ( $\text{NO}_3^- + 6\text{H}_2\text{O} + 8\text{e}^- \rightarrow \text{NH}_3 + 9\text{OH}^-$ ). First, the solubility of sodium nitrate ( $880 \text{ g L}^{-1}$ ) is significantly higher than that of  $\text{N}_2$  in water ( $20 \text{ mg L}^{-1}$ ), transforming the gas-liquid-solid tri-phase heterogeneous catalysis into a two-phase process. More importantly, the dissociation of single and double bonds between N and O in  $\text{NO}_3^-$  needs far less energy ( $48.7 \text{ kcal mol}^{-1}$ ) compared to the  $\text{N}\equiv\text{N}$  triple bond, which has an extremely strong bond dissociation energy ( $225 \text{ kcal mol}^{-1}$ ).<sup>52–55</sup> In terms of energy input, contact electrification and triboelectrification offer effective means of conducting interfacial redox reactions, capitalizing on renewable energy sources such as wind, tide, and water evaporation.<sup>45–48</sup> The charge separation will occur across the interfaces of the gas, solid, and liquid phases, which possess different abilities in capturing electrons or protons, providing the electric potential difference that drives various chemical reactions.

The air interface region of microbubbles and microdroplets provides a redox-active microenvironment that enables the direct activation of ambient nitrogen and oxygen, producing ROS such as  $\text{OH}^\cdot$ ,  $\text{O}_2^-$ , and singlet oxygen ( $^1\text{O}_2$ ).<sup>37,38</sup> These air-water interfacial redox properties can be further enhanced through collaboration with photocatalysis and contact electrocatalysis. PTFE nanoparticles and a molecular iron-based photocatalyst were introduced into the reaction system to maximize the nitrate production from air in the first critical step. Ultrasonicating PTFE dispersion can be the pre-production step to provide extra  $\text{H}_2\text{O}_2$  on the baseline level of ROS generated by microbubbles. Iron is an ideal metal to incorporate into a photocatalyst. First, it can absorb solar radiation to activate triplet oxygen into singlet status ( $^3\text{O}_2 \rightarrow ^1\text{O}_2$ ), which is highly reactive and can be converted to superoxide by capturing free electrons ( $^1\text{O}_2 + \text{e}^- \rightarrow \text{O}_2^-$ ). This process can be well coupled with the single electron transfer process occurring across the microbubble interfacial region ( $\text{OH}^- \rightarrow \text{OH}^\cdot + \text{e}^-$ ). On the other hand, the iron-center porphyrin photocatalyst also allows a Fenton-like reaction, which can break the relatively stable  $\text{H}_2\text{O}_2$  into more reactive  $\text{OH}^\cdot$  for  $\text{N}_2$  oxidation.<sup>56–58</sup>

Iron oxide-based catalysts have shown significant activity in electrocatalytic hydrogen evolution reactions (HERs), effectively promoting water splitting and generating active hydrogen species ( $^*\text{H}$ ), which are essential for the hydrogenation steps in the  $\text{NO}_3\text{RR}$ .<sup>57</sup> Compared to copper-based catalysts, iron oxides exhibit stronger affinity for nitrite ( $\text{NO}_2^-$ ) intermediates, enhancing their further reduction to ammonia.<sup>58</sup> A porous CuO mesh-supported  $\text{Fe}_3\text{O}_4\text{-Nafion}$  catalyst demonstrates improved  $\text{NO}_3^-$  adsorption and electron transfer due to the synergistic interaction between Cu and Fe active sites, which weakens the



N–O bonds and lowers the activation energy barrier. In this tandem system, Cu primarily facilitates the reduction of  $\text{NO}_3^-$  to  $\text{NO}_2^-$ , while  $\text{Fe}_3\text{O}_4$  catalyzes the subsequent hydrogenation to  $\text{NH}_3$ . The introduction of a microdroplet interface further amplifies the process by providing a large electric field, as well as a high interfacial surface area, which enhances mass transport and concentrates  $\text{NO}_x$  intermediates and  $\text{H}^+$  species. Overall, the combination of tandem catalysis and interfacial microdroplet dynamics enables efficient and selective nitrate-to-ammonia conversion under ambient aqueous conditions.

Ammonium nitrate ( $\text{NH}_4\text{NO}_3$ ) is a commonly used nitrogen fertilizer that provides both  $\text{NH}_4^+$  and  $\text{NO}_3^-$ , two essential forms of nitrogen that plants readily absorb. Its balanced application is critical for optimal plant development, as excess nitrate can contribute to environmental issues including groundwater contamination, whilst too much ammonium can induce osmotic stress and toxicity in sensitive crops.<sup>50</sup> This is especially crucial in controlled situations such as hydroponics, where accurate nutrient management is required. A concentration range of 1 to 3  $\text{mM L}^{-1}$  ammonium nitrate<sup>51</sup> is typically suitable for hydroponic plant seedlings and other controlled hydroponic farming systems. This range ensures that the plants receive sufficient nitrogen without causing osmotic stress. Our current method of synthesis can reliably achieve this concentration range, demonstrating its effectiveness and feasibility. This means that the suggested method can be used to produce ammonium nitrate on-site, *in situ*, regularly, ensuring a sustainable supply. This makes it a valuable method for managing nutrients in hydroponic systems, providing both long-lasting and precise control.

The energy input is contributed by photon energy stemming from solar irradiation, electric energy for running a diaphragm pump, and kinetic energy released from the compressed gas in cylinder, generating microbubbles and microdroplets to create a more reactive air–water interface area. We conducted an estimation of these three sources of energy consumption within 12 hours of micro-bubbling stage and 1 hour of microdroplet spraying stage (Tables S1–S3). As a result, electronic energy only accounts for 6% of the total energy, and the kinetic energy stored from the compressed gas cylinder can be negligible (less than 1%). Because solar energy can be regarded as a free source, and kinetic energy can be negligible, the price of  $\text{HNO}_3$  and  $\text{NH}_3$  is calculated by dividing the cost of electricity with generated product weights. The calculation results show US \$5.98 per gram  $\text{HNO}_3$  and US \$126.4 per gram  $\text{NH}_3$  (Table S4). Compared to the ammonia's global market price around US \$0.00047 per gram and nitric acid's price of approximately US \$ 0.00038 per gram, we acknowledge that the cost of the present method is still not competitive with the HBP from the point of view of energy cost. Nonetheless, this method still provides the potential solution that has advantages in replacing fossil energy with carbon-free, clean energy from the point of view of environmental protection.

To further improve the production efficiency and lower the energy cost, the larger-scale bubbling system is still under investigation, which will be independent work in near future. First, a larger volume microbubble reactor should be

introduced to increase the amount of dinitrogen gas to be oxidized. The interfacial nitrogen oxidation time can also be extended by raising the height of the bulk water surface. The microbubble density can be increased by replacing a single microbubble generator with a generator array. Dinitrogen molecules can be more effectively dispersed and oxidized by generating nano-sized bubbles. Given these measures, we believe that the produced nitrate can reach over hundreds of mM and even the M level at the gallon scale.

## Conclusion

We have demonstrated an air–water interfacial redox approach to produce mM-level ammonium nitrate under ambient conditions, reducing the requirement for energy-intensive processes involved in traditional ammonia and nitric acid production. Such decentralized and ecologically friendly solutions not only lower carbon footprints but also enable scalable and site-specific fertilizer generation, which is critical for sustainable food production in a changing climate.

## Author contributions

X. S., C. B., and R. N. Z. conceptualized the research idea about the interfacial nitrogen cycle. X. S. and C. B. conducted methodology development. X. S., C. B., and J. X. constructed the prototype. X. S. collected the nitrate production data by using mass spectrometry. C. B. collected the ammonia concentration data from the UV-vis colorimetry test. J. X. collected the nitrate concentration data by ion chromatography. C. B. and R. N. Z. supervised the whole research progress. X. S. wrote the original draft. C. B. and R. N. Z. revised and finalized the draft.

## Conflicts of interest

For R. N. Z., C. B., and X. S., a patent disclosure has been made to the Stanford Office of Technology Licensing: expedited chemical reactions at curved microscale interfaces between water and a hydrophobic medium. PCT application number PCT/US2024/012974 filed 25 January 2024. The other authors declare that they have no competing interests.

## Data availability

All data needed to evaluate the conclusions in the paper are present in the paper and/or the supplementary information (SI). Supplementary information is available. See DOI: <https://doi.org/10.1039/d5sc05754j>.

## Acknowledgements

The authors acknowledge financial support from the Stanford Sustainability Accelerator Program (GHG-0030) (R. N. Z.), Air Force Office of Scientific Research through the Multidisciplinary University Research Initiative program (AFOSR FA9550-21-1-0170) (R. N. Z.), KFUPM International Summer Research



Program (ISP241-CHEM-829) (C. B.), and Deanship of Research at KFUPM (ER221003) (C. B.).

## References

- J. W. Erisman, M. A. Sutton, J. Galloway, Z. Klimont and W. Winiwarter, How a century of ammonia synthesis changed the world, *Nat. Geosci.*, 2008, **1**(10), 636–639.
- V. Smil, *Enriching the Earth: Fritz Haber, Carl Bosch, and the Transformation of World Food Production*, MIT Press, 2004.
- H. Iriawan, S. Z. Andersen, X. Zhang, B. M. Comer, J. Barrio, P. Chen, A. J. Medford, I. E. Stephens, I. Chorkendorff and Y. Shao-Horn, Methods for nitrogen activation by reduction and oxidation, *Nat. Rev. Methods Primers*, 2021, **1**(1), 56.
- D. R. MacFarlane, P. V. Cherepanov, J. Choi, B. H. Suryanto, R. Y. Hodgetts, J. M. Bakker, F. M. F. Vallana and A. N. Simonov, A roadmap to the ammonia economy, *Joule*, 2020, **4**(6), 1186–1205.
- C. Smith, A. K. Hill and L. Torrente-Murciano, Current and future role of Haber–Bosch ammonia in a carbon-free energy landscape, *Energy Environ. Sci.*, 2020, **13**(2), 331–344.
- M. Capdevila-Cortada, Electrifying the Haber–Bosch, *Nat. Catal.*, 2019, **2**(12), 1055.
- X. Yuan, D. Zhang, C. Liang and X. Zhang, Spontaneous reduction of transition metal ions by one electron in water microdroplets and the atmospheric implications, *J. Am. Chem. Soc.*, 2023, **145**(5), 2800–2805.
- L. Zhao, X. Song, C. Gong, D. Zhang, R. Wang, R. N. Zare and X. Zhang, Sprayed water microdroplets containing dissolved pyridine spontaneously generate pyridyl anions, *Proc. Natl. Acad. Sci. U. S. A.*, 2022, **119**(12), e2200991119.
- X. Song, Y. Meng and R. N. Zare, Spraying water microdroplets containing 1,2,3-triazole converts carbon dioxide into formic acid, *J. Am. Chem. Soc.*, 2022, **144**(37), 16744–16748.
- H. Chen, R. Wang, T. Chiba, K. Foreman, K. Bowen and X. Zhang, Designer “Quasi-Benzynes”: The spontaneous reduction of ortho-diiodotetrafluorobenzene on water microdroplets, *J. Am. Chem. Soc.*, 2024, **146**(15), 10979–10983.
- J. K. Lee, D. Samanta, H. G. Nam and R. N. Zare, Micrometer-sized water droplets induce spontaneous reduction, *J. Am. Chem. Soc.*, 2019, **141**(27), 10585–10589.
- S. Jin, H. Chen, X. Yuan, D. Xing, R. Wang, L. Zhao, D. Zhang, C. Gong, C. Zhu, X. Gao and Y. Chen, The spontaneous electron-mediated redox processes on sprayed water microdroplets, *JACS Au*, 2023, **3**(6), 1563–1571.
- C. K. Weatherly, M. W. Glasscott and J. E. Dick, Voltammetric analysis of redox reactions and ion transfer in water microdroplets, *Langmuir*, 2020, **36**(28), 8231–8239.
- J. P. Heindel, R. A. LaCour and T. Head-Gordon, The role of charge in microdroplet redox chemistry, *Nat. Commun.*, 2024, **15**(1), 3670.
- X. Yuan, D. Zhang, C. Liang and X. Zhang, Spontaneous reduction of transition metal ions by one electron in water microdroplets and the atmospheric implications, *J. Am. Chem. Soc.*, 2023, **145**(5), 2800–2805.
- M. A. Mehrgardi, M. Mofidfar and R. N. Zare, Sprayed water microdroplets are able to generate hydrogen peroxide spontaneously, *J. Am. Chem. Soc.*, 2022, **144**(17), 7606–7609.
- L. E. Krushinski and J. E. Dick, Direct electrochemical evidence suggests that aqueous microdroplets spontaneously produce hydrogen peroxide, *Proc. Natl. Acad. Sci. U. S. A.*, 2024, **121**(12), e2321064121.
- R. Xie, K. Guo, Y. Li, Y. Zhang, H. Zhong, D. Y. Leung and H. Huang, Harnessing air-water interface to generate interfacial ROS for ultrafast environmental remediation, *Nat. Commun.*, 2024, **15**(1), 8860.
- L. Qiu and R. G. Cooks, Spontaneous oxidation in aqueous microdroplets: water radical cation as primary oxidizing agent, *Angew. Chem.*, 2024, **136**(17), e202400118.
- T. Majumder, D. B. Eremin, B. Delibas, A. Sarkar, V. Fokin and J. M. Dawlaty, Calibrating the oxidative capacity of microdroplets, *Angew. Chem., Int. Ed.*, 2024, e202414746.
- Z. Rao, X. Li, Y. G. Fang, J. S. Francisco, C. Zhu and C. Chu, Spontaneous oxidation of thiols and thioether at the air-water interface of a sea spray microdroplet, *J. Am. Chem. Soc.*, 2023, **145**(19), 10839–10846.
- S. F. Nami-Ana, M. A. Mehrgardi, M. Mofidfar and R. N. Zare, Sustained regeneration of hydrogen peroxide at the water–gas interface of electrogenerated microbubbles on an electrode surface, *J. Am. Chem. Soc.*, 2024, **146**(46), 31945–31949.
- X. Song, Y. Wan, Q. Yang, J. Zhang, Y. Zhang, Z. Sun, S. Li, J. Zhang, X. Zhang, S. Ciampi and L. Zhang, Electrode Fouling by Gas Bubbles Enables Catalyst-Free Hydrogen Peroxide Synthesis, *J. Am. Chem. Soc.*, 2025, **147**(26), 22864–22872.
- X. Song, C. Basheer and R. N. Zare, Making ammonia from nitrogen and water microdroplets, *Proc. Natl. Acad. Sci. U. S. A.*, 2023, **120**(16), e2301206120.
- X. Song, C. Basheer, J. Xu and R. N. Zare, Onsite ammonia synthesis from water vapor and nitrogen in the air, *Sci. Adv.*, 2024, **10**(50), eads4443.
- A. Kumar, V. S. Avadhani, A. Nandy, S. Mondal, B. Pathak, V. K. N. Pavuluri, M. M. Avulapati and S. Banerjee, Water microdroplets in air: A hitherto unnoticed natural source of nitrogen oxides, *Anal. Chem.*, 2024, **96**(26), 10515–10523.
- Y. Wang, J. Luo, Y. G. Fang, Z. A. Nan, X. Cui, T. Chen, X. Zeng, X. Wang, X. Song, J. Zhao and W. Li, Catalyst-free nitrogen fixation by microdroplets through a radical-mediated disproportionation mechanism under ambient conditions, *J. Am. Chem. Soc.*, 2025, **147**(3), 2756–2765.
- S. Bose, M. Mofidfar and R. N. Zare, Direct conversion of N<sub>2</sub> and air to nitric acid in gas–water microbubbles, *J. Am. Chem. Soc.*, 2024, **146**(40), 27964–27971.
- S. Bose, Y. Xia and R. N. Zare, Understanding the formation of nitrate from nitrogen at the interface of gas–water microbubbles, *Chem. Sci.*, 2024, **15**(47), 19764–19769.
- X. Song, C. Basheer, Y. Xia and R. N. Zare, Oxidation of ammonia in water microdroplets produces nitrate and molecular hydrogen, *Environ. Sci. Technol.*, 2024, **58**(36), 16196–16203.
- K. Li, B. Zhang, D. Xia, Z. Ye, Y. Pan, J. S. Francisco and Z. Mi, Room-Temperature Catalyst-Free Ammonia Decomposition



- for Hydrogen Production on Water Microdroplets, *J. Am. Chem. Soc.*, 2025, **147**(24), 20417–20425.
- 32 X. Song, C. Basheer, J. Xu, M. M. Adam and R. N. Zare, Methane Bubbled Through Seawater Can be Converted to Methanol With High Efficiency, *Advanced Science*, 2025, **12**(10), 2412246.
- 33 J. Li, J. Xu, Q. Song, X. Zhang, Y. Xia and R. N. Zare, Methane C (sp<sup>3</sup>)-H bond activation by water microbubbles, *Chem. Sci.*, 2024, **15**(41), 17026–17031.
- 34 J. Zhao, X. Zhang, J. Xu, W. Tang, Z. Lin Wang and F. Ru Fan, Contact-electro-catalysis for direct synthesis of H<sub>2</sub>O<sub>2</sub> under ambient conditions, *Angew. Chem., Int. Ed.*, 2023, **62**(21), e202300604.
- 35 W. Li, J. Sun, M. Wang, J. Xu, Y. Wang, L. Yang, R. Yan, H. He, S. Wang, W. Q. Deng and Z. Q. Tian, Contact-electro-catalysis for direct oxidation of methane under ambient conditions, *Angew. Chem.*, 2024, **136**(20), e202403114.
- 36 A. J. Colussi, Mechanism of hydrogen peroxide formation on sprayed water microdroplets, *J. Am. Chem. Soc.*, 2023, **145**(30), 16315–16317.
- 37 J. Zhou, Q. Wang, G. Cheng, W. Shen, R. N. Zare and X. Sun, Charged Water Microdroplets Enable Dissociation of Surrounding Dioxygen, *J. Am. Chem. Soc.*, 2025, **147**(13), 10916–10924.
- 38 F. Li, J. Lv, A. He, J. Xu, L. Zhao, X. Wang, L. Mao, S. Li, H. Wang, Y. Wang and G. Jiang, Unexpected Generation of Singlet Oxygen at the Air–Water Interface of Aqueous Microdroplets, *J. Am. Chem. Soc.*, 2025, **147**(34), 30574–30581.
- 39 K. Li, Q. Ge, Y. Liu, L. Wang, K. Gong, J. Liu, L. Xie, W. Wang, X. Ruan and L. Zhang, Highly efficient photocatalytic H<sub>2</sub>O<sub>2</sub> production in microdroplets: accelerated charge separation and transfer at interfaces, *Energy Environ. Sci.*, 2023, **16**(3), 1135–1145.
- 40 W. Wang, Y. Liu, T. Wang, Q. Ge, K. Li, J. Liu, W. You, L. Wang, L. Xie, H. Fu and J. Chen, Significantly accelerated photosensitized formation of atmospheric sulfate at the air–water interface of microdroplets, *J. Am. Chem. Soc.*, 2024, **146**(10), 6580–6590.
- 41 K. Li, K. Gong, J. Liu, L. Ohnoutek, J. Ao, Y. Liu, X. Chen, G. Xu, X. Ruan, H. Cheng and J. Han, Significantly accelerated photochemical and photocatalytic reactions in microdroplets, *Cell Rep. Phys. Sci.*, 2022, **3**(6), 100917.
- 42 Q. Gao, B. Yao, H. S. Pillai, W. Zang, X. Han, Y. Liu, S. W. Yu, Z. Yan, B. Min, S. Zhang and H. Zhou, Synthesis of core/shell nanocrystals with ordered intermetallic single-atom alloy layers for nitrate electroreduction to ammonia, *Nat. Synth.*, 2023, **2**(7), 624–634.
- 43 S. Han, H. Li, T. Li, F. Chen, R. Yang, Y. Yu and B. Zhang, Ultralow overpotential nitrate reduction to ammonia via a three-step relay mechanism, *Nat. Catal.*, 2023, **6**(5), 402–414.
- 44 Y. Wang, M. Sun, J. Zhou, Y. Xiong, Q. Zhang, C. Ye, X. Wang, P. Lu, T. Feng, F. Hao and F. Liu, Atomic coordination environment engineering of bimetallic alloy nanostructures for efficient ammonia electrosynthesis from nitrate, *Proc. Natl. Acad. Sci. U. S. A.*, 2023, **120**(32), e2306461120.
- 45 Z. L. Wang, T. Jiang and L. Xu, Toward the blue energy dream by triboelectric nanogenerator networks, *Nano Energy*, 2017, **39**, 9–23.
- 46 C. Wu, A. C. Wang, W. Ding, H. Guo and Z. L. Wang, Triboelectric nanogenerator: a foundation of the energy for the new era, *Adv. Energy Mater.*, 2019, **9**(1), 1802906.
- 47 B. Chen, Y. Yang and Z. L. Wang, Scavenging wind energy by triboelectric nanogenerators, *Adv. Energy Mater.*, 2018, **8**(10), 1702649.
- 48 S. Fang, W. Chu, J. Tan and W. Guo, The mechanism for solar irradiation enhanced evaporation and electricity generation, *Nano Energy*, 2022, **101**, 107605.
- 49 Y. Meng, Y. Xia, J. Xu and R. N. Zare, Spraying of water microdroplets forms luminescence and causes chemical reactions in surrounding gas, *Sci. Adv.*, 2025, **11**(11), eadt8979.
- 50 J. Shilpha, J. Song and B. R. Jeong, Ammonium phytotoxicity and tolerance: An insight into ammonium nutrition to improve crop productivity, *Agronomy*, 2023, **13**(6), 1487.
- 51 Z. Yang, H. Yan, H. Liu, L. Yang, G. Mi and P. Wang, Enhancing crop nitrogen efficiency: the role of mixed nitrate and ammonium supply in plant growth and development, *Biology*, 2025, **14**(5), 546.
- 52 X. Li, Y. Yang, Q. Ding and Y. Wang, Recent advances in Fe, Mo-based electrocatalysts for nitrogen reduction under ambient conditions, *Sustainable Energy Fuels*, 2024, **14**, 3020–3035.
- 53 X. Meng, K. Wang, Z. Zhao, K. Li, W. Sun and Y. Lin, Preventing nitrite desorption via switching hydrogenation position: a dual-site approach for selective nitrate reduction to ammonia, *Small*, 2025, **21**, 2407216.
- 54 H. Zhang, H. Wang, X. Cao, M. Chen, Y. Liu, Y. Zhou, M. Huang, *et al.*. Unveiling cutting-edge developments in electrocatalytic nitrate-to-ammonia conversion, *Adv. Mater.*, 2024, **36**, 2312746.
- 55 W. Tian, H. Guo, T. Li, S. Luo, S. Tian and Y. Zhou, In-situ characterization techniques for electrochemical nitrate-to-ammonia conversion, *Sustainable Energy Fuels*, 2025, **9**, 4507.
- 56 L. G. Devi, M. L. ArunaKumari, B. G. Anitha, R. Shyamala and G. Poornima, Photocatalytic evaluation of Hemin (chloro(protoporphyrinato)iron(III)) anchored ZnO hetero-aggregate system under UV/solar light irradiation: A surface modification method, *Surf. Interfaces*, 2016, **1**, 52–58.
- 57 H. Yi, M. Jiang, D. Huang, G. Zeng, C. Lai, L. Qin, C. Zhou, B. Li, X. Liu, M. Cheng and W. Xue, Advanced photocatalytic Fenton-like process over biomimetic hemin-Bi<sub>2</sub>WO<sub>6</sub> with enhanced pH, *J. Taiwan Inst. Chem. Eng.*, 2018, **93**, 184–192.
- 58 C. Xu, L. Zhou, S. Zheng, D. Yu, Y. Tang, C. Fan, C. Lin, D. Zhou and Y. Lin, Hemin covalently functionalized carbon nanobranch with enzyme-like and photocatalytic activities for synergistic dye degradation and antibacterial therapy, *Adv. Sustainable Syst.*, 2021, **5**(9), 2100103.

